An experimentally-based modeling study of the effect of anti-angiogenic therapies on primary tumor kinetics for data analysis of clinically relevant animal models of metastasis

Aristoteles Camillo

Université Pierre et Marie Curie
Master de Sciences & Technologies
M2 Mathématiques & Applications
Rapport de stage - Master 2

Advisors:
Jorge P. Zubelli & Sébastien Benzekry

An experimentally-based modeling study of the effect of anti-angiogenic therapies on primary tumor kinetics for data analysis of clinically relevant animal models of metastasis

Aristoteles Camillo

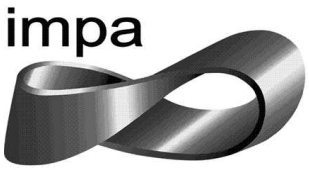

February, 2014 - August, 2014

Contents

Remerciements

Je voudrais adresser mes plus sincères remerciements :

À Sébastien, plus que mon tuteur, un ami qui m'a accompagné tout au long de ces six mois et qui m'a introduit dans le monde des maths appliquées à la biologie.

À Jorge qui a fait tout son possible pour que je travaille dans les meilleures conditions à mon retour au Brésil.

À Sarah une grande amie qui m'a beaucoup aidé dans l'écriture de ce rapport en faisant des remarques pertinentes sur la clarté des informations exposées ainsi que des corrections d'anglais. Son soutien a été de très grande importance.

Je voulais remercier l'équipe Inria MC2 et en particulier Thierry Colin ainsi que l'université de Bordeaux pour m'avoir accueilli pendant mon stage.

Je remercie aussi John Ebos (Roswell Park Cancer Institute, Buffalo, NY, USA) de nous avoir fourni les données et détails expérimentaux.

Enfin, ce stage a reçu le soutien financier du programme "Investissements pour le futur" de IdEx Bordeaux - CPU (ANR-10-IDEX-03-02) pour lequel je suis reconnaissant.

Introduction

Metastasis are responsible of 90% of the deaths of patients with solid cancer disease (see [Gupta and Massagué, 2006]). In the scientific literature, many mathematical models are reported to describe the primary tumor evolution. In order to help clinicians making choices regarding to the treatment of cancer patients with metastatic disease, we also need mathematical models which evaluate the metastatic state of the patient and compare the efficacy of some anti-cancerous drugs.

To obtain additional informations about the evolution of the metastatic process, we test several existing growth models on the data from experiments in tumor-bearing mice to select those able to describe the dynamic of an untreated tumor and take into account the effect of both anti-angiogenic (AA) and cytotoxic drugs. Iwata proposed in 2000 a simple model which depicts the primary tumor and the metastéasis dynamics. However, it does not take into account the angiogenesis process which is what the Benzekry's thesis (see [Benzekry, 2011]) is about: combining in a theoretical approach, the Iwata model with the tumor growth model introduced by Hahnfeldt and al. (see [Hahnfeldt et al., 1999]). Even if the ultimate goal of this study is about taking into account metastasis evolution, my work ensures the first step: numerical validation of tumor growth models on the primary tumor.

Concurrently, recent developments in cancer biology allowed experimentalists to develop clinically relevant *in vivo* systems that mimick the development of metastases ([Ebos et al., 2009]). These animal models are intended to evaluate the efficacy of anti-cancerous drugs not only on the primary tumor (which is the most widely spread usage) but also (and more importantly in a (neo-)adjuvant context) on the development of metastases. These are monitored by non-invasive techniques based on bioluminescence. In collaboration with experimentalists from the Roswell Park Cancer Institute in Buffalo, NY, USA (John Ebos' lab), we have at our disposal a set of data from experiments with untreated mice and treated ones with an AA oral administration. In the chapter 2, some well-known models are tested on the first group of experimental data (on untreated mice), assessing the models according to various criteria (goodness of fit and normalized standard error). The model parameters used in the next step were also obtained thanks to the fits to the average of the vehicle group.

The treated groups received an oral administration of Sunitinib following different schedulings. In chapter 3, the first problem we had to resolve was the absence of an explicit pharmacokinetic (PK) model for the Sunitinib dynamic in mice. So before comparing the treated data and the models, we tested a PK model which matched the experiments data of the mice Sunitinib concentration. It allowed us to test the models which integrate the AA effect on treated tumor-bearing mice. Indeed, we studied their descriptive power and their predictive power (from one scheduling, being able to capture other schedulings).

Chapter 1

Presentation of the biological and mathematical problems

1.1 Oncology backgrounds

About clinical oncology

This disease is characterized by an abnormal cell growth (unregulated growth) in a normal tissue. It starts with one or several healthy cells in which appear some genetic mutations that are transmitted to next generations losing more and more normal cell properties. There are also two kinds of tumor: benign or malignant. To differentiate it, Hanahan and Weinberg proposed six characteristics of **malignancies**:

1. Self-sufficiency in growth signalling.
2. Insensitivity to anti-growth signals.
3. Evasion of apoptosis.
4. Enabling of a limitless replicative potential.
5. Induction and sustainment of angiogenesis.
6. Activation of metastasis and invasion of tissue.

The mass could grow until 2-3mm of diameter without any nutrient supply (oxygen, glucose, etc.). Folkman discovered that at this point, the cells send signals to stimulate the formation of a vascular network surrounding the tumor (see [Folkman, 1971]). This process is called **neo-angiogenesis**, it's provoked by molecules such as the **Vascular Endothelial Growth Factor (VEGF)** emitted from the primary tumor.

It is the first step to the development of secondary tumors (**metastasis**). Indeed, cancer cells detach from the primary tumor and through the blood vessels migrate to other tissues (liver, lungs, kidneys...) see Figure 1.1.

Anti-angiogenic treatments

Thanks to Folkman's observations, a new strategy of therapy of solid tumor is considered by inhibiting the growth of new blood vessels which starve the tumor cells (decrease of nutrient

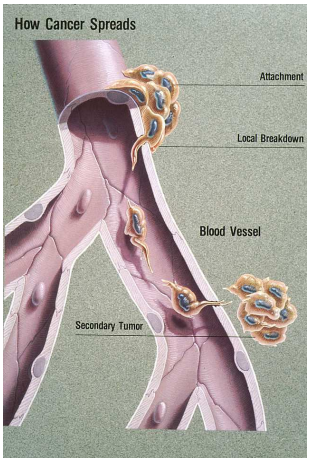

Figure 1.1: Metastatic dissemination

supply). There are two widely used angiogenesis inhibitors:

- Tyrosine Kinase Inhibitors which bind the VEGF receptors avoiding activation of intracellular pathways of proliferation and migration.
- Monoclonal antibodies which bind the VEGF molecules and inactive them.

This kind of treatment called **cytostatic therapy** is opposed to a **cytotoxic treatment** with a direct tumor cell kill effect.

1.2 Mathematical modeling

Iwata derived a transport equation for the metastatic population distribution structured by a physical trait X which can represent for example the size[1] (V) or/and the vascularization (K) of the tumor. We make the assumption that the primary tumor is generated at time $t = 0$ by a single cell. Primary tumor and metastases grow with rate $G(t, X)$ and emit new metastases at rate $\beta(X)$ (see Figure 1.2). Let $\rho(t, X)$ represent the population distribution structured by the trait X at time t. This model writes

$$\begin{cases} \partial_t \rho(t,X) + div(\rho(t,X)G(t,X)) = 0, & \forall X \in \Omega, \quad t \geq 0 \\ -G(t,\sigma).\nu\rho(t,\sigma) = N(\sigma)\{\int_\Omega \beta(X)\rho(t,X)dX + \beta(X_p(t))\}, & \sigma \in \partial\Omega, t \geq 0, \\ \rho(0,X) = 0 & X \in \Omega \end{cases} \tag{1.1}$$

Where X_p represents the primary tumor trait which satisfies the ODE $\dot{X}_p(t) = G(t, X_p(t))$ and N is the distribution of metastases at birth.

We can derive from ρ, the solution of the previous system of equation, some useful quantities:

$$\text{Total number of metastasis} = \int_\Omega \rho(t,X)dX,$$
$$\text{Metastatic burden} = \int_\Omega X\rho(t,X)dX,$$

A natural and important question comes out of the equation (1.1): what model(s) do we use for the tumor growth function (G)? A first one, proposed by Iwata and al in their publication, is the Gompertz law. In the following chapters, we propose to test some other known models

[1] either express in number of cells or mm^3, using the conversion rule $1mm^3 \simeq 10^6 cells$

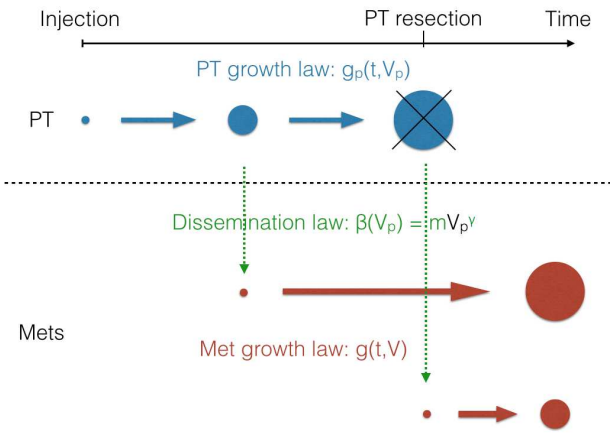

Figure 1.2: Schema of the Model (see [Benzekry et al., 2014a])

(Power Law, Dynamic CC, Exponential-linear) on our data of untreated primary tumor. Then, we integrate the AA therapy in those growth models and compare them to the data of treated primary tumor.

1.3 Animal model

Human metastatic breast cancer 231/LM2-4LUC+ cells expressing luciferase were injected into the tail vein of severe combined immunodeficiency (SCID) mice, which then received vehicle treatment or sunitinib therapy regimen administered by gavage after tumor cell inoculation (Figure 1.1). Bioluminescence have been used to monitorate tumor growth. These experiments have been reported in [Ebos et al., 2009].

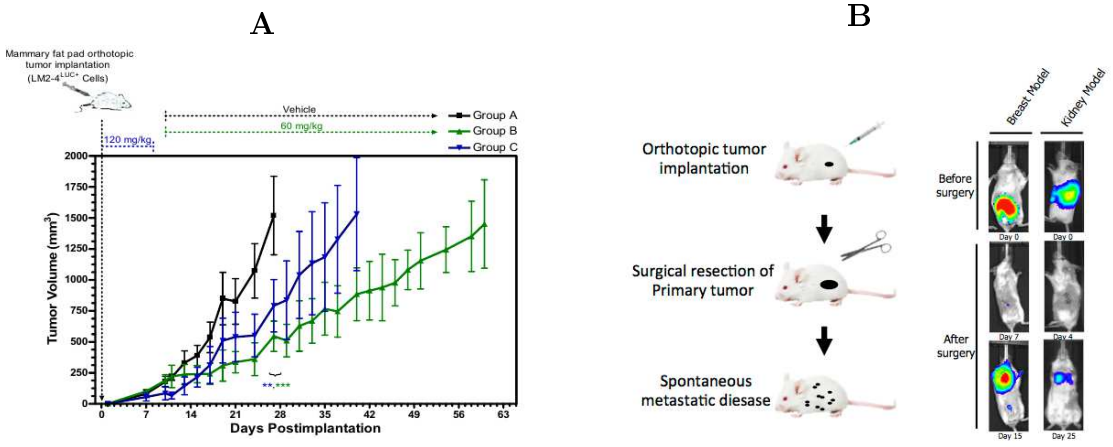

Table 1.1: Animal models of metastases: (A) [Ebos et al., 2009] (B) [Ebos et al., 2014]

Chapter 2

Tumor growth without treatment

2.1 Models

All the models describe the total tumor volume growth. As a function of time the tumor volume is denoted $V(t)$. The proportion between the total number of cells in the tumor and the tumor volume is translated by the conversion rule $1mm^3 \simeq 10^6$ cells. In the interest of reduce the degrees of freedom, for all models but the Gompertz V_0, we fix the initial value $V_0 = 1mm^3$, as in [Benzekry et al., 2014b].

Exponential-Linear model

This model supposes that tumor growth has two phases:

1. a **exponential growth**: cells proliferate with a constant rate $a_0 = \ln(2/T_C)$ where T_C is the constant cell cycle length;
2. a **linear growth**: where a_1 is its slope.

Giving the following formation,

$$\begin{cases} \frac{d}{dt}V(t) = a_0 V, & t \leq \tau \\ \frac{d}{dt}V(t) = a_1, & t \geq \tau \\ V(t=0) = V_0 \end{cases} \tag{2.1}$$

It is convenient to express this behavior using the following single differential equation:

$$\begin{cases} \frac{d}{dt}V(t) = \frac{a_0 V(t)}{[1+(\frac{a_0}{a_1}V(t))^{\psi}]^{\frac{1}{\psi}}} \\ V(t=0) = V_0 \end{cases} \tag{2.2}$$

where ψ is a shape factor ($\psi = 20$ is our choice) based in [Simeoni et al., 2004].

Assuming that the solution of the Cauchy problem is continuously differentiable, τ is determinated by $\tau = \frac{1}{a_0}\log(\frac{a_1}{a_0 V_0})$.

Gompertz model

It belongs to a family of models that asymptotically converges to a maximal value, the carrying capacity. As a limit case of the generalized logistic model, its mean characteristic is its exponential decay of the growth rate. The two formulation of this model are useful.

- The Cauchy problem for the volume:

$$\begin{cases} \frac{d}{dt}V(t) = ae^{-\beta t}V(t) \\ V_0 = 27.9mm^3 \end{cases} \tag{2.3}$$

  where V_0 is fixed to the value of this parameter in the average fit;

- The analytic formula:

$$V(t) = V_0 e^{\frac{a}{\beta}(1-e^{-\beta t})}$$

Where a is the initial proliferation rate and β is the rate of exponential decay of the proliferation rate.

In the analytic formula we can easily see that asymptotically the total tumor volume converges to $V_0 e^{\frac{a}{\beta}}$, the carrying capacity.

Gompertz V_0 model

In this model, we offer one more degree of freedom to the Gompertz, not fixing the initial value V_0.

$$\frac{d}{dt}V(t) = ae^{-\beta t}V(t)$$

Power Law model

This model claims that the tumor growth is proportional to the number of proliferative cells (supposing that they have a constant cell cycle length). It suggests that the proliferative tissue is proportional to V^γ as we can see in the following formulation:

$$\begin{cases} \frac{d}{dt}V(t) = aV^\gamma \\ V(t=0) = V_0 \end{cases} \tag{2.4}$$

Where γ can be interpreted as a possible fractional Hausdorff dimension of the proliferative tissue, when viewed as a metric subspace of the full tumor volume.

Dynamic CC model

This model integrates a dynamic to the carrying capacity K. Assuming that K represents the tumor vascularization and that it is proportional to the tumor surface. This dynamic is given by :

$$\begin{cases} \frac{d}{dt}V(t) = aV(t)\log(\frac{K(t)}{V(t)}) \\ \frac{d}{dt}K(t) = bV(t)^{2/3} \\ V(t=0) = V_0; \quad K(t=0) = K_0 \end{cases} \tag{2.5}$$

It can be noticed that this model is very useful to integrate an anti-angiogenic treatment as it takes into account the vascularization dynamic, where cytostatic treatment takes place (see Chapter 3).

2.2 Goodness of fit relevance in a population study

The goal of this section is in a first time to elect some models which are able to describe and predict the evolution of a breast carcinoma without treatment in an experimental mouse model. We could ingenuously think that goodness of fit criteria are sufficient to make this analysis, nevertheless if we are also interested in a model's ability to take into account inter-animal variability, it is not enough.

At our disposal, we have six separate experiments which monitor the primary tumor's growth after an orthotopic tumor implantation (Figure 2.1). Even if we fitted our models to each group, in this report, we focus on group 3 where we have at our disposal different schedulings to a AA treatment.

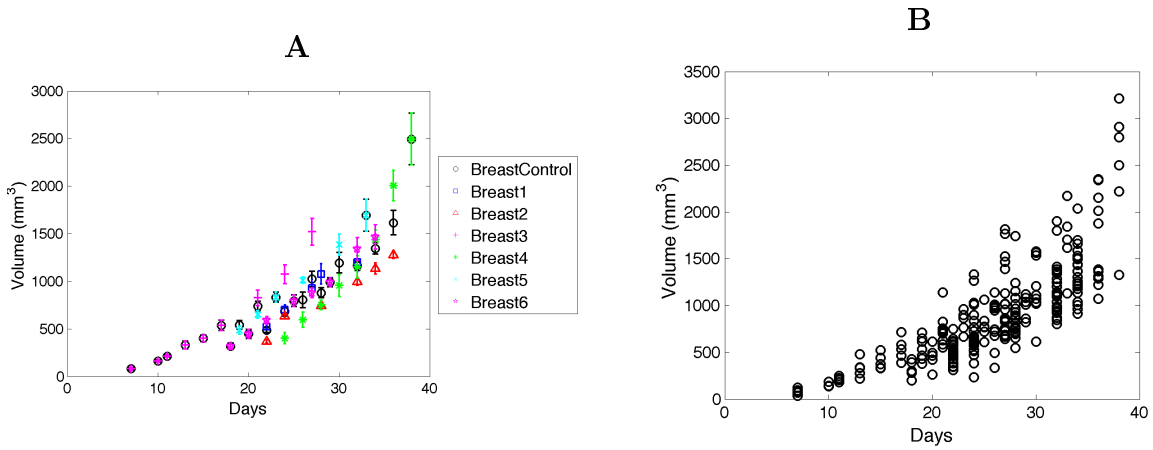

Table 2.1: (A) Average growth of all vehicle groups (B) Brut data set (*Breast Control*)

2.2.1 Individual approach

Fitting a model to each animal within the population, we obtain different parameter sets. To take this inter-animal variability into account, we make here the same assumption as [Benzekry et al., 2014b]: for each model, parameters are realization of a random variable taken to be log-normally distributed. Following this individual approach, we estimate a global distribution of the model parameters in the vehicule group 3. The median and coefficient of variation are reported in Table 2.2.

Parameters of group 3

Model	Par.	Unit	Median value (CV)	NSE (%) (CV)
Gompertz V_0	α	$[day^{-1}]$	0.433 (24.1)	33.5 (24.2)
	β	$[day^{-1}]$	0.0696 (30)	33 (20.7)
	V_0	$[mm^3]$	7.08 (79.9)	80.4 (36.9)
Power law	a	$\left[mm^{3(1-\gamma)} \cdot day^{-1}\right]$	1.81 (31.8)	13.6 (16.2)
	γ	-	0.578 (11.1)	5.1 (25.8)
Dynamic CC	a	$[day^{-1}]$	0.836 (173)	19.8 (68.4)
	b	$[mm^{-2} \cdot day^{-1}]$	1.2 (15.8)	8.69 (39.2)
Gompertz	α	$[day^{-1}]$	0.846 (9.51)	5.08 (24.2)
	β	$[day^{-1}]$	0.113 (12.7)	7.85 (25.4)
Exponential-linear	a_0	$[day^{-1}]$	0.518 (11.2)	5.86 (149)
	a_1	$[mm^3 \cdot day^{-1}]$	53.4 (30)	12.3 (49.5)

Table 2.2: Shown are the median values within the population and in parenthesis the coefficient of variation (CV, expressed in percent and defined as the standard deviation within the population divided by mean and multiplied by 100) that quantifies inter-animal variability. Last column represents the normalized standard errors (NSE) of the maximum likelihood estimator, defined in [Benzekry et al., 2014b].

To validate this hypothesis in our data, for each growth model we simulated 1000 growth curves assuming that parameters are like above. Then we plotted the median, the first decile and the last decile of this *in silico* population (Table 2.3). This is extremely useful to interpret the data in Table 2.2.

The deciles are not supposed to contain all data points, they must capture the population scattering. Comparing all the models, the Gompertz V_0 does not describe the population as well as the others, which is caused by its high CV in parameters. In other experimental groups of mice, it is even clearer: its higher CV produces deciles definitely too wide. However, the high variance within the population on the parameter a to the Dynamic CC does not preclude this model capturing the population scattering. From visual examination, the other models seem to describe tumor growth within the vehicle group in an accurate fashion.

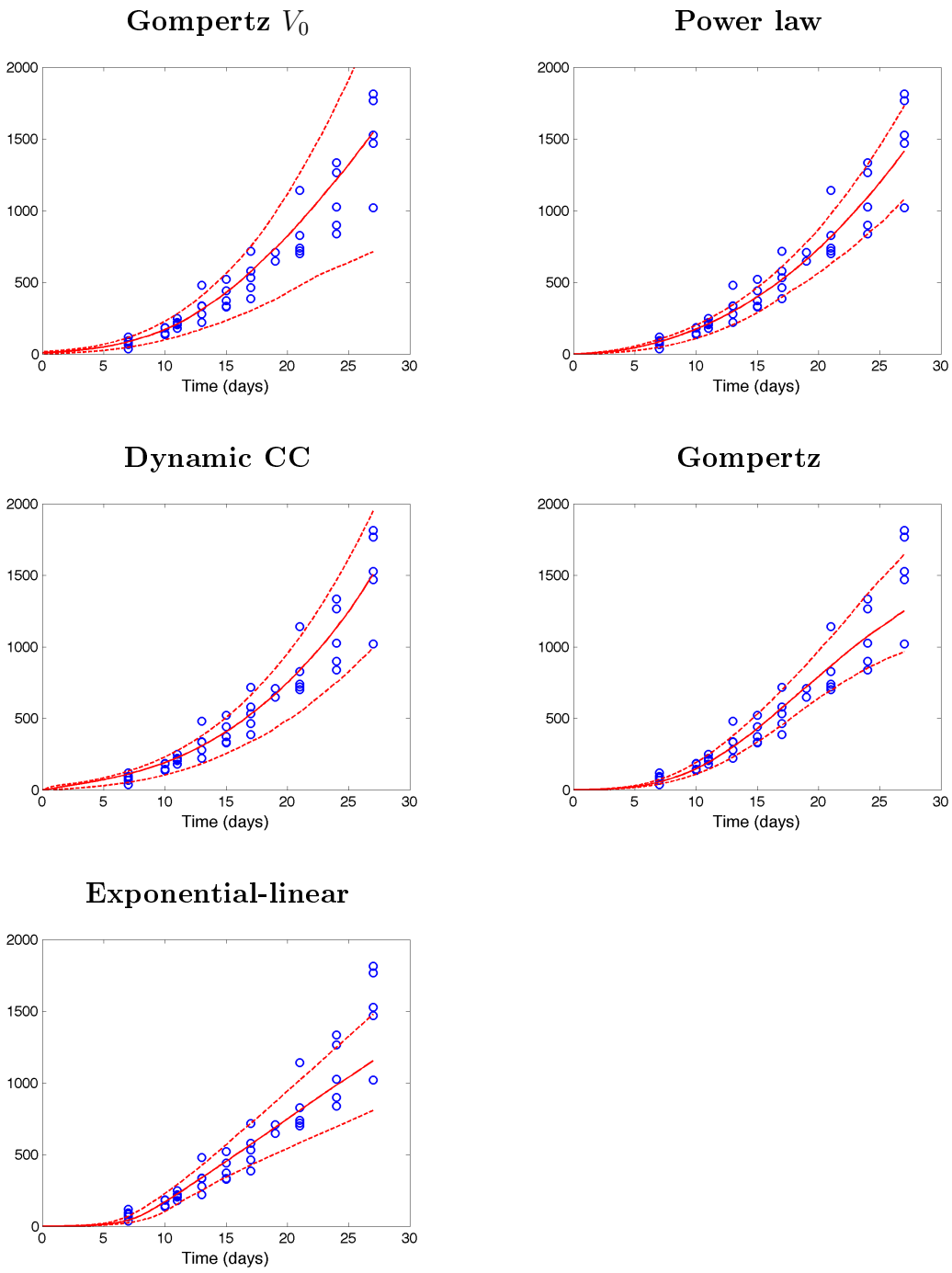

Table 2.3: Median (*continuous line*) and deciles (*broken line*) of a *in silico* population as defined above compared to experimental data.

This approach is very relevant when we do not have many data points. In the individual approach, the parameters distribution penalizes the sum of squared residual following the equation (21) of [Benzekry et al., 2014b] in parameters estimation. It makes it possible to find the parameters which are near to data and to the median value at the same time, it balances the lack of information. Nevertheless, to our study (group 3) we have enough data points to adopt an average approach. It reduces the complexity of the study without be deprived of precision.

2.2.2 Average approach

Pure goodness of fit is not enough to judge the descriptive power of a model since parameter parsimony is also important. High number of parameters are responsible for identifiability issues. To counterbalance the importance of pure goodness of fit, we have at our disposal other metrics that penalize high number of parameters (for example, the RMSE and the AIC). For more details, see [Benzekry et al., 2014b].

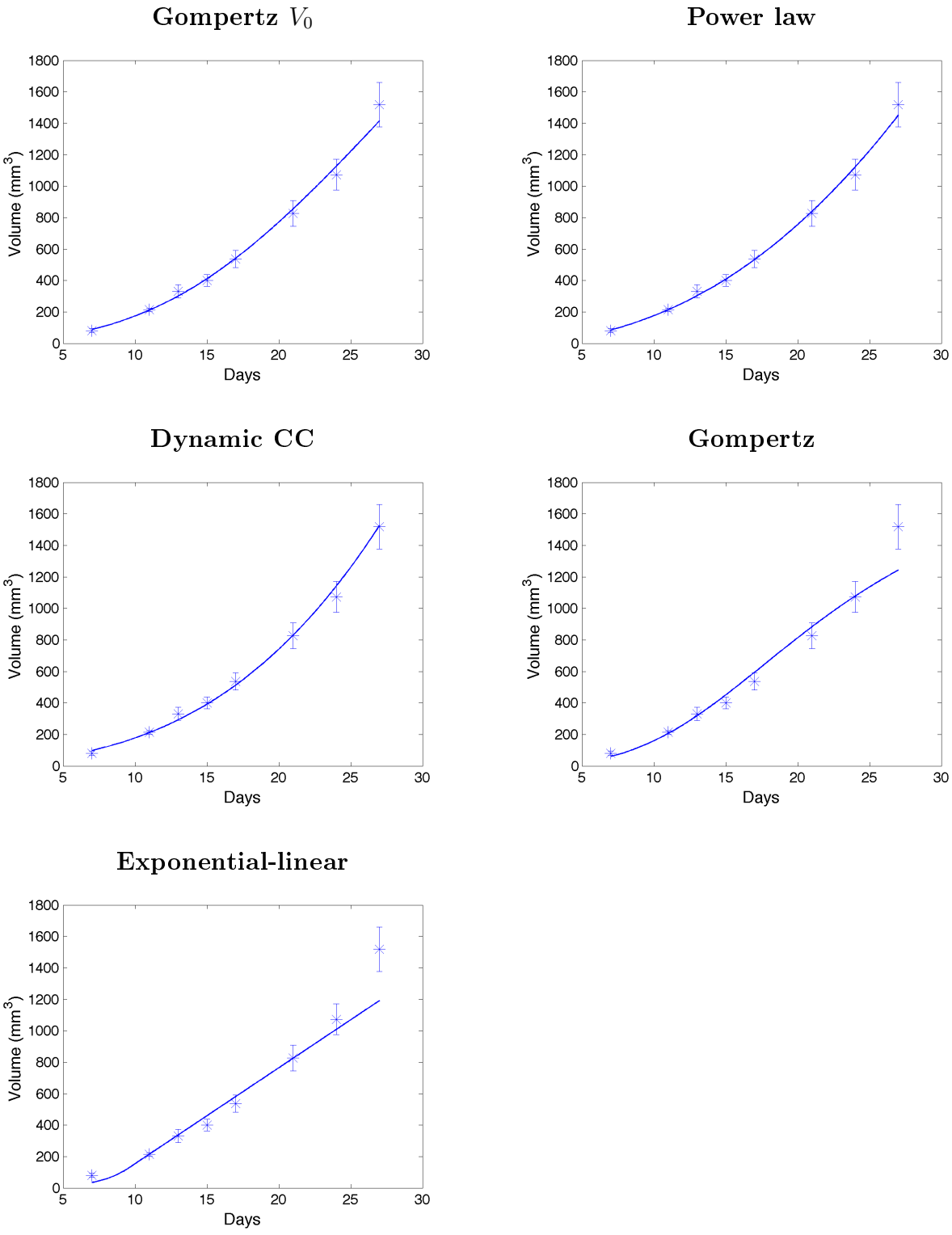

Table 2.4: Data (*symbols*) and model-fitted (*solid lines*) tumor growth curves obtained in tumor-bearing mice.

When analyzing the Goodness of fit, the Power Law (two parameters model) model has surprisingly the best performance whereas the Gompertz (three parameters model) is ranked second in all criterias. The AIC of Gompertz is significantly different from the AIC of the Power Law (> 2) due to a double penalization: not a better fit than the Power Law and an additional degree of freedom.

This being said, all models successfully depict tumor growth with the Exponential-Linear that show a somewhat poorer descriptive power as the linear phase of this model does not match closely the breast tumor growth.

Goodness of fit of models for the vehicule group 3

Model	**SSE**	**RMSE**	**AIC**	#
Power law	**0.00953[1]**	**0.104[1]**	**-31.2[1]**	2
Gompertz V_0	0.0141[2]	0.123[2]	-26.1[2]	3
Dynamic CC	0.0332[3]	0.194[3]	-21.2[3]	2
Gompertz	0.0824[4]	0.304[4]	-14[4]	2
Exponential-linear	0.148[5]	0.405[5]	-9.27[5]	2

Table 2.5: Models were ranked in ascending order of the RMSE. For each metric, indicated are the mean value (among all animals) and in parenthesis the minimal and maximal values. When reported, value inside brackets is the rank of the model for the underlying metric. The model ranking first is highlighted in bold. # is the number of parameters. This table presentation and parameters are the same used by Benzekry in [Benzekry et al., 2014b].

Parameters of the average data on group 3

Model	Par.	Unit	Value	SE (%)
Power law	a	$[mm^{3(1-\gamma)} \cdot day^{-1}]$	1.92	4.95
	γ	-	0.567	1.99
Gompertz V_0	α	$[day^{-1}]$	0.423	13.9
	β	$[day^{-1}]$	0.0693	13.4
	V_0	$[mm^3]$	8	30.7
Dynamic CC	a	$[day^{-1}]$	0.884	16.1
	b	$[mm^{-2} \cdot day^{-1}]$	1.2	5.73
Gompertz	α	$[day^{-1}]$	0.868	4.8
	β	$[day^{-1}]$	0.117	6.84
Exponential-linear	a_0	$[day^{-1}]$	0.612	19.1
	a_1	$[mm^3 \cdot day^{-1}]$	47.7	19.7

Table 2.6:

Since Gompertz V_0 additional degree of freedom is responsible for its poor identifiability of parameters (rather high SE, see Table 2.6), the Gompertz should thus be preferred as it is also able to depict the tumor growth dynamic and is identifiable.

As a remark, it is interesting to notice the proximity of results between the individual approach and the average approach. It supports our decision to continue our study fitting models on average data.

Taken together, our results show that the two parameters models are good compromises between the goodness of fit and the number of parameters. In the next chapter, we fix the parameters to the average ones. Then, we integrate the AA treatment term in those models in order to fit them on experiments with treated cancer-bearing mice. And we focus our discussion on the drug's efficacy.

Chapter 3

Anti-angiogenic treatment

The sunitinib acts on the tumor vascularization: it inhibits the action of the Vascular Endothelial Growth Factor (VEGF) molecule which is responsible for the neo-angiogenesis. The result of its action is not the direct cell kill but it deprives the tumor of oxygen and nutrients inhibiting the proliferation of the surrounding blood vessels.

3.1 Growth model considering the angiogenic dynamic

Model of Hahnfeldt et al. ([Hahnfeldt et al., 1999])

Hahnfeldt et al. were one of the first who proposed a model depicting the tumor growth under the angiogenic influence in the article [Hahnfeldt et al., 1999]. It is very useful when we want to evaluate the evolution of a tumor growth under a AA therapy.

It is an extension of some Gompertz law ($G(t,V) = aV\ln(K/V)$) considering the carrying capacity K no more as a constant parameter but as a dynamic variable representing the tumor vascularization. It makes sense since the vascularization limits the tumor growth. Indeed, it regulates the nutrient supply to the tumor. They derived the vascularization dynamic taking into account: stimulation (*via* molecules such as VEGF) and inhibition (through angiogenesis inhibitors such as endostatin and angiostatin, see [O'Reilly et al., 1994]) of the vascularization by the tumor itself. After their numerical analysis, they deduced that the inhibition concentration is proportional to the radius of the tumor to the square. They came up with the following equation:

$$\begin{cases} \frac{d}{dt}V(t) = aV(t)\ln(\frac{K(t)}{V(t)}) \\ \frac{d}{dt}K(t) = cV(t) - dV(t)^{\frac{2}{3}}K(t) \end{cases} \tag{3.1}$$

The AA therapy is integrated in the model through a death term in the equation for K in the system (2.3) which becomes:

$$\frac{d}{dt}K(t) = cV(t) - dV(t)^{\frac{2}{3}}K(t) - e_{AA}C(t)K(t)$$

with $C(t)$ is the plasma concentration of the drug and e_{AA} the efficacy parameter.

In that article, the authors estimated the value of the parameter e_{AA} and the pharmacokinetic parameter (which allows to compute $C(t)$) for three AA drugs (edostatin, angiostatin and TNP-470). They fixed the growth parameters using the ones fitted for the tumor growth without treatment.

In the Annexe A.1, we reported those values and plotted the volume and the tumor vascularization under different AA treatments in order to observe the control of the vascularization on the tumor growth.

For our study, we also fix the growth parameters from the untreated mice data calculated in section 2. However, instead of fitting the pharmacokinetic parameters on treated tumor growth as they did due to a lack of information, we succeeded in analyzing the sunitinib pharmacokinetics thanks to kinetics studies of this drug allowing us to confront a pharmacokinetic model to biological data.

3.2 Pharmacokinetics of Sunitinib

In order to study the sunitinib efficacy, we can not ignore the dynamic of this drug in the mice body. Each substance has a different fate between its administration and its elimination in a living organism. In this section, we propose to study the pharmacokinetic (defined in [Gunaratna, 2001] as the quantitative study of the time course of drug absorption, distribution, metabolism and elimination.) of an intravenous and oral administration of sunitinib. In order to simplify the processes that take place in the interaction between an organism and this drug, we adopt an one-compartment model (see Figure 3.1) for both kind of administration.

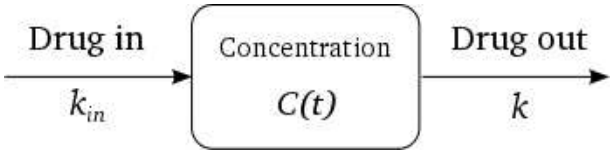

Figure 3.1: One-compartment model

3.2.1 The PK in an intravenous administration

Since intravenously administrated drugs are distributed very rapidly throughout the body without an absorption step, we just have to considerate its elimination. Thus here we consider that the elimination rate of sunitinib follows first order kinetics (it decreases as the drug concentration drops). Under these assumptions, sunitinib concentration after a single intravenous administration can be described by :

$$C(t) = \frac{D}{V_d} e^{-kt} \tag{3.2}$$

Where k is its first order constant, D the dose and V_d the volume of distribution (for an interpretation of this pharmacokinetic parameters, see [Gunaratna, 2001]).

Unfortunately, to verify our assumptions, we did not find in the pharmacological literature any experiments showing the evolution in time of sunitinib concentration in mice for an intravenous dosing. Nevertheless, in [Haznedar et al., 2009] the sunitinib concentrations in rats and monkeys after a bolus administration of this drug have been monitored. Subsequently, despite the

biological differences between mice and rats, we consider that the rat PK and the mice PK are similar. In our study, we thus integrate in the tumor growth models the PK parameters of rats.

PK models confrontation

From [Haznedar et al., 2009], we have $t_{1/2}$ and V_d for different intravenous dosing in rats. The correspondence between $t_{1/2}$ and k is given by $t_{1/2} = \frac{\ln(2)}{k}$.

Dose (mg/kg)	$t_{1/2}$(h)	V_d(L/Kg)
1	1.9	9.3
4	2.1	5.5
8	2.3	3.9
4	2.5	4.6

Table 3.1: PK parameters of sunitinib in rats from [Haznedar et al., 2009]

	$t_{1/2}$(h)	k (1/h)	V_d(L/Kg)
Average	2.3	0.301	4.7

Table 3.2: PK average parameters

Adding to this, we also have experimental data that monitored the evolution of the sunitinib concentration following intravenous dosing of 10 mg/kg to which we fitted the one-compartment model (see Figure 3.2).

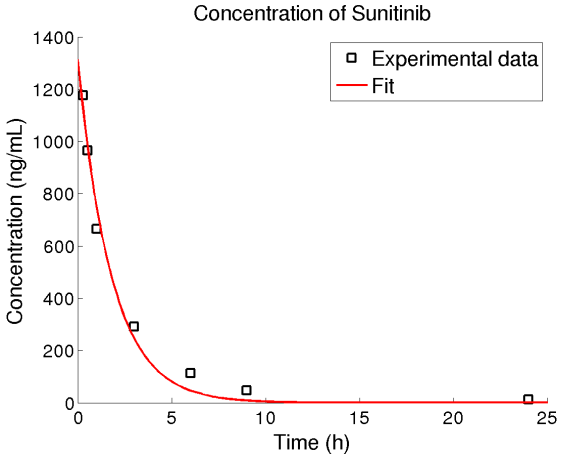

Figure 3.2: Plasma concentration of sunitinib following intravenous dosing in rats (10 mg/kg) and fit curve.

$t_{1/2}$(h)	k (1/h)	V_d (L/kg)
1.24	0.557	3.043

Table 3.3: PK parameters from fit to intravenous data

Since the comparison between the PK parameters from literature and the ones from our fit (Table 3.3) is satisfactory, it was not an ingenuous assumption considering a one-compartment model to an intravenous administration of sunitinib.

However, we can not forget the variability of PK parameters. Indeed, we remark that even for the same dose, we find two different V_d (in Table 3.1). Moreover we know that the apparent volume of distribution is independent of the drug concentration. To respect this assumption, we can take the average of these values except the first one (too big compared to the others).

As we can see in Figure 3.3, integrating the average of PK parameters from literature (see Table 3.2) in the one-compartment model reproduces quite well the evolution of the plasma concentration of the sunitinib for a 10 mg/kg intravenous administration. Using the average PK parameters thus is a good compromise to evaluate the sunitinib concentration after an intravenous administration into rats.

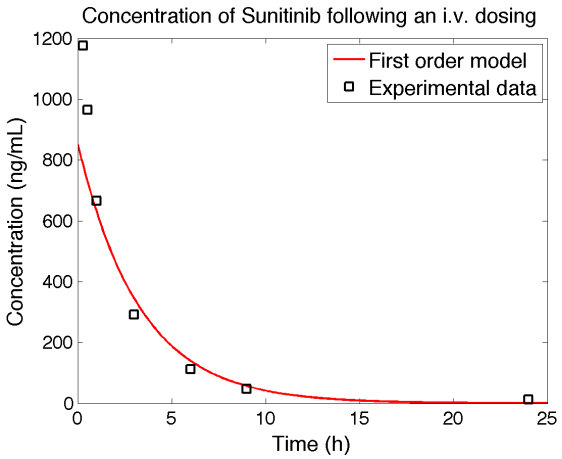

Figure 3.3: Plasma concentration of sunitinib following intravenous dosing in rats (10 mg/kg) and first order kinectics simulating the same experiment using the average PK parameters.

3.2.2 The PK in an oral administration and confrontation to experimental data

In Haznedar's study plasma pharmacokinetic parameters of sunitinib after an oral administration were analyzed using non-compartment methods. Unfortunately these methods do not describe the time course of the drug in the blood.

A gavage administration involves an absorption step. The change in plasma drug concentration will now be a function of both the absorption rate k_{in} and elimination rate k. In the one-compartment model concentration's expression is given by:

$$C(t) = \frac{Dk_{in}}{V_d(k_{in} - k)}(e^{-kt} - e^{-k_{in}t})$$

In this section we do not use the Haznedar pharmacokinetic parameters. Instead, we fit the one-compartment model to their data of plasma concentration of sunitinib after an oral administration of 4 mg/kg (see Figure 3.4).

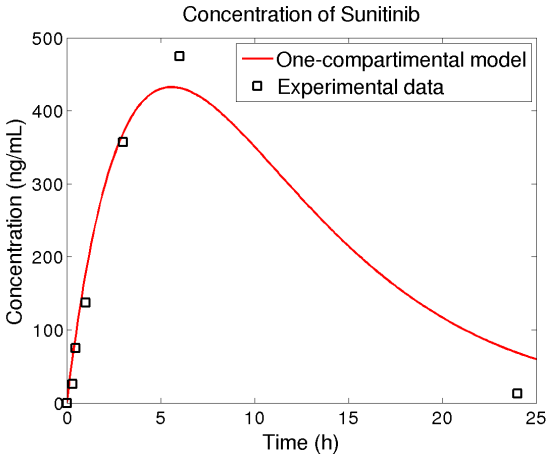

Figure 3.4: Plasma concentration of sunitinib after oral administration in rats (4 mg/kg) and fit curve.

k_{in} (1/h)	k (1/h)	V_d (L/kg)
0.1793	0.1794	8.5039

Table 3.4: PK parameters from fit to oral administration data

In the next section, we will use these PK parameters (see Table 3.4) into tumor growth models which are able to integrate the AA treatment. Indeed, we are interested in the efficacy of the sunitinib.

3.3 Pharmacodynamic modeling of tumor growth after administration of Sunitinib

To take the action of the AA treatments into account in the models able to predict the primary tumor growth, we don't make a cell kill hypothesis, but we implement the effect of anti-angiogenic compounds using an inhibitory effect on the growth functions (as Rocchetti et al. described it for a single-agent experiment in [Rocchetti et al., 2013]). Indeed, the sunitinib is part of a cytostatic therapy, as opposed to a cytotoxic treatment (classical chemotherapy).

3.3.1 PK-PD model structures

The anti-angiogenic tumor growth inhibition (TGI) models

Assuming that the anti-angiogenic drug acts as an inhibitor on the tumor growth, without a cell kill effect, we introduce a new term in the previous models as following:

Simeoni AA TGI

$$\begin{cases} \frac{d}{dt}V(t) = \frac{a_0 V(t)}{[1+(\frac{a_0}{a_1}V(t))^{\psi}]^{\frac{1}{\psi}}}[1 - \frac{C_{AA}(t)}{C_{AA}(t)+IC_{50}}] \\ V(t=0) = V_0 \end{cases} \tag{3.3}$$

Gompertz AA TGI

$$\begin{cases} \frac{d}{dt}V(t) = a\exp^{-\beta t}V(t)[1 - \frac{C_{AA}(t)}{C_{AA}(t)+IC_{50}}] \\ V(t=0) = V_0 \end{cases} \tag{3.4}$$

Power Law AA TGI

$$\begin{cases} \frac{d}{dt}V(t) = aV^{\gamma}[1 - \frac{C_{AA}(t)}{C_{AA}(t)+IC_{50}}] \\ V(t=0) = V_0 \end{cases} \tag{3.5}$$

Where IC_{50} parameter represents the concentration of the drug that inhibits by 50% the maximal tumor growth. Smaller it is, faster the therapy term is near zero which means that the tumor stops growing. So we could use it as a representative of the drug efficiency. Remark that when the anti-angiogenic is eliminated, the tumor growth rate reverts back to the rate before treatment.

We can also add the anti-angiogenic treatment to the Dynamic CC model. It is not a difficult task thanks to the model's nature which takes into account the vascularization dynamic (K).

Dynamic CC AA

$$\begin{cases} \frac{d}{dt}V(t) = aV(t)\log(\frac{K(t)}{V(t)}) \\ \frac{d}{dt}K(t) = bV(t)^{2/3} - e_{AA}C_{AA}(t) \\ V(t=0) = V_0; \quad K(t=0) = K_0 \end{cases} \tag{3.6}$$

Where the e_{AA} represents the drug efficacy.

3.3.2 Results

At our disposal, we have two sets of treated tumor-bearing mice (see Table 1.1):

- *BreastSub31* received a sustained sunitinib therapy (60 mg/kg) when tumors reached an average volume of 200 mm^3.
- *BreastSub32* received a short-term sunitinib therapy (120 mg/kg during 7 days) starting the day after tumor implantation.

To fit our models to these data, the tumor growth parameters were first identified from the vehicule group (see Table 2.6) and the PK parameters were fixed from those estimated in the section 3.2.2. We now are able to focus our attention to the efficacy parameters of the drug (IC_{50} and e_{AA}).

Model	SSE	RMSE	AIC	#
Dyn CC AA	**1.79[1]**	**1.34[1]**	**18[1]**	1
Gomp AA	8.6[2]	2.99[2]	55.6[2]	1
Power Law AA	11.8[3]	3.43[3]	63.2[3]	1
Simeoni AA	14.9[4]	3.87[4]	68.8[4]	1

Table 3.5: Goodness of Fit of BreastSub31

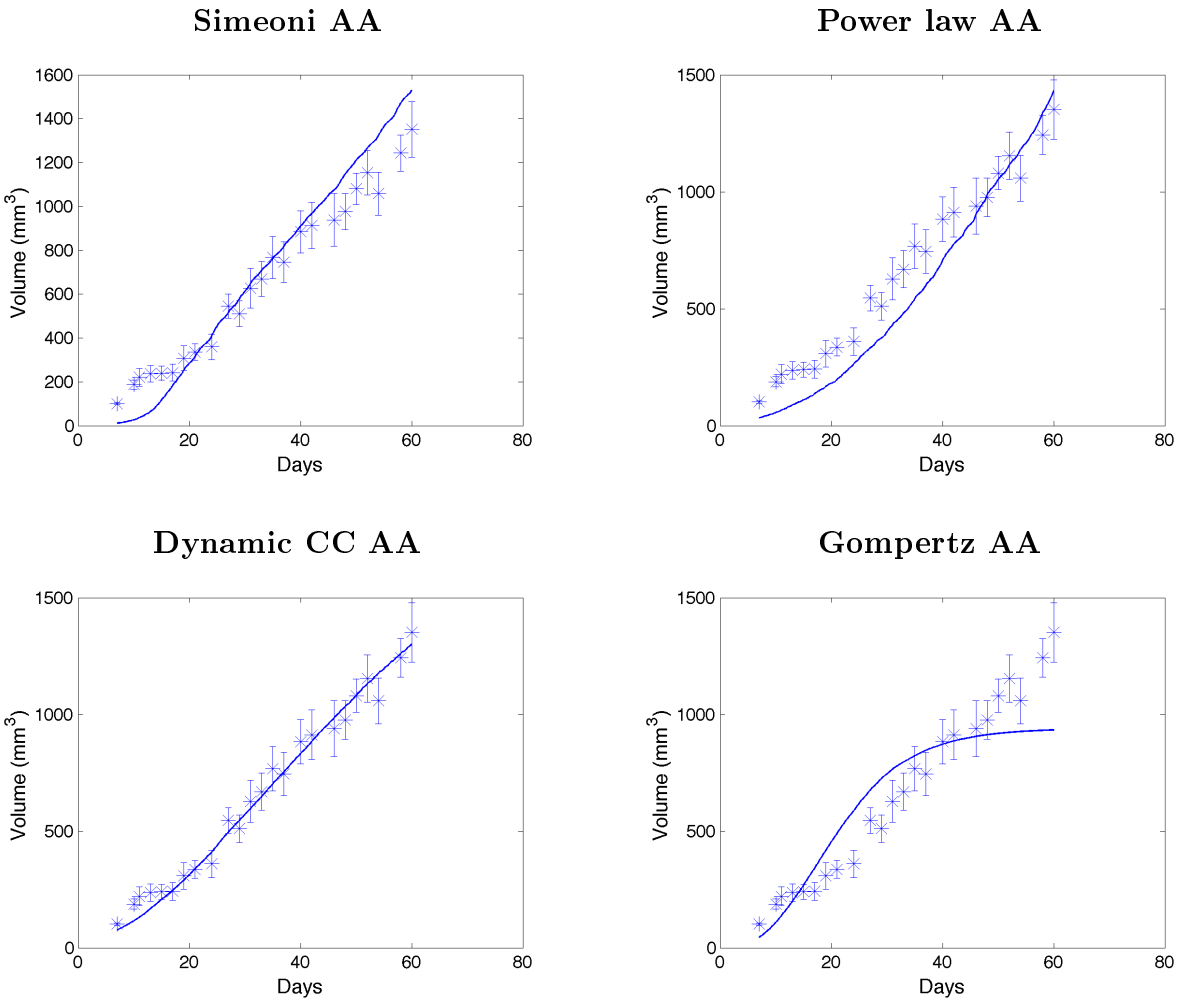

Table 3.6: Fits to *BreastSub31*

Model	SSE	RMSE	AIC	#
Gomp AA	3.2[2]	**1.79[1]**	21.5[2]	1
Simeoni AA	**3[1]**	1.79[2]	**20.5[1]**	1
Power Law AA	3.79[3]	2.02[3]	24[3]	1
Dyn CC AA	31.9[4]	5.84[4]	55.9[4]	1

Table 3.7: Goodness of Fit of BreastSub32

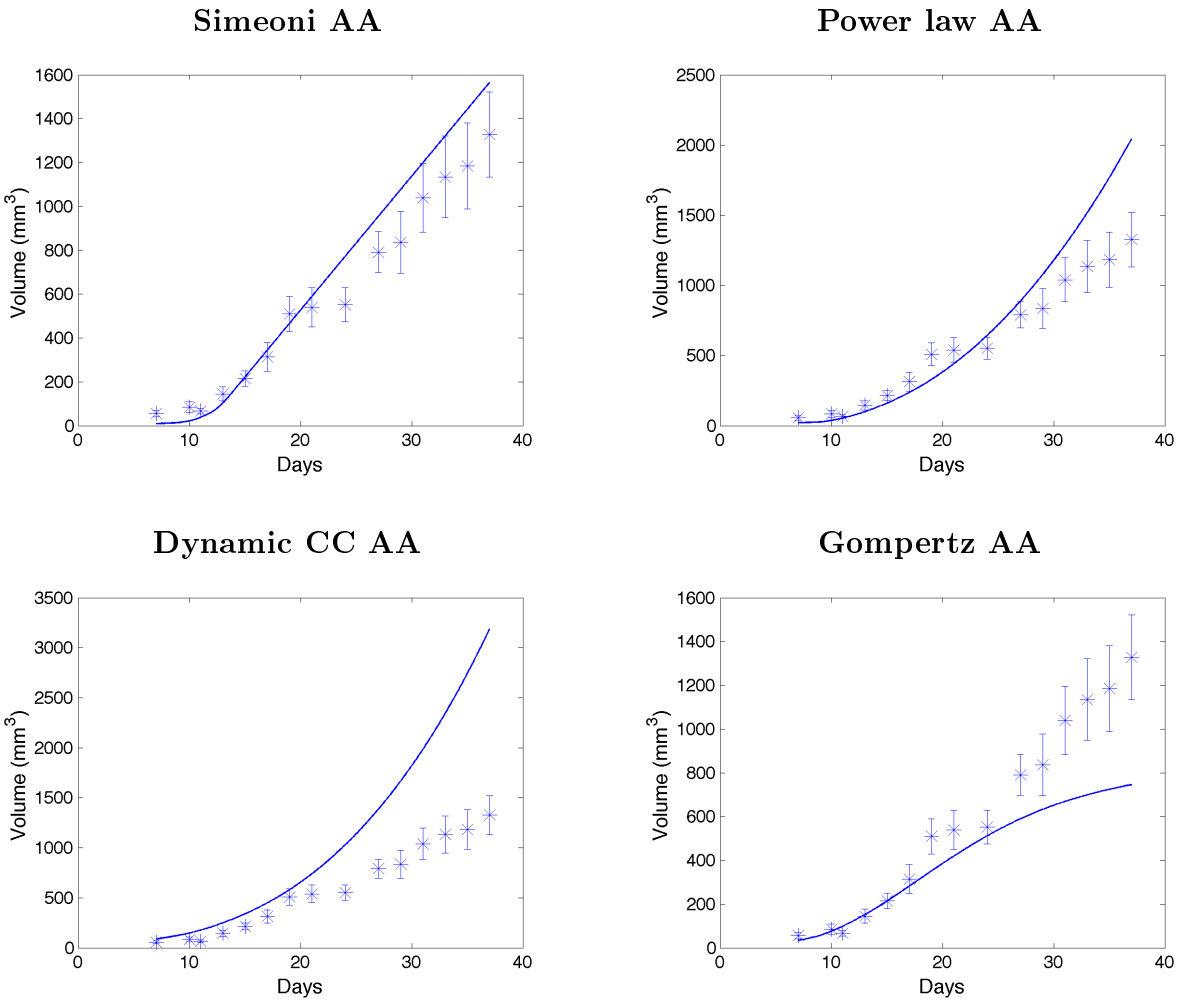

Table 3.8: Fits to *BreastSub32*

Descriptive power

First of all, from a visual examination of Table 3.6 the Gompertz AA TGI did not well explain the tumor growth of the treated breast group *BreastSub31*. In the Table 3.8, we see that the Power law AA TGI, Gompertz AA TGI and the Dynamic CC AA are unable to predict the *BreatSub32* tumor growth dynamic. At last, the Simeoni AA TGI successfully describes the curves of the treated groups.

These analyzes were surprisingly not confirmed by goodness of fit criterias (see Tables 3.5 and 3.7). For example, in Table 3.5, the Gompertz AA TGI which clearly does not follow the curve of data on the graph arrived at the second place above the Simeoni AA TGI which understood better the dynamic of the tumor growth with treatment. It is interesting to notice that both analyzes furnish informations to judge the relevance of a model because they point at different model characteristics. However, in this particular case, the contradiction between the visual examination and the performance examination brings us to prefer the graphs rather than the goodness of fit criterias to make our selection.

At this point, we reject all the models but the Simeoni AA TGI which describes in both groups the tumor growth with AA treatment in a reasonably accurate fashion. In the next paragraph, we will be interesting in evaluating the predictive power of this model.

Predictive power

To study the predictive power of the Simeoni AA model, those experiments data of different schedulings are considered. The growth parameters are those identified from the vehicle group. And the efficacy parameter IC_{50} used to predict the tumor growth of the *BreastSub31* is the one fitted to *BreastSub32* (See Table 3.9).

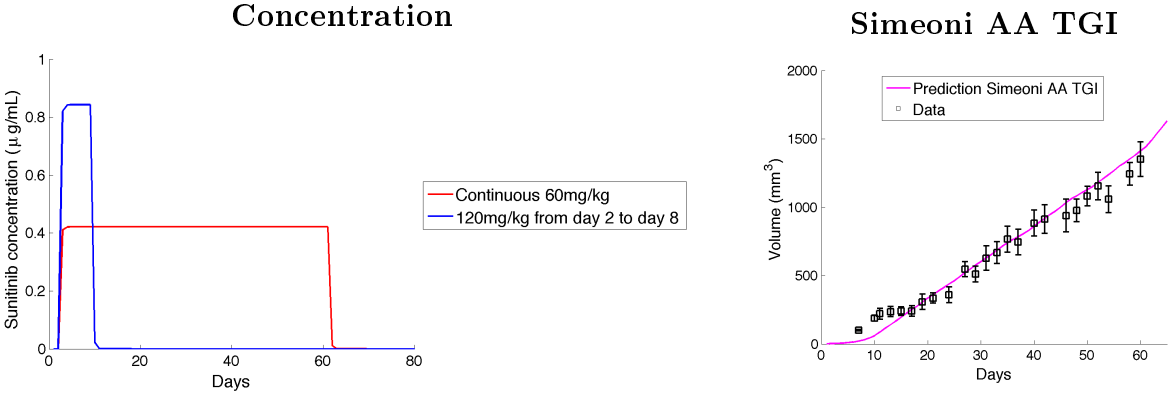

Table 3.9: Predictive power of AA models on *BreastSub31*

			BreastSub31		BreastSub32	
Model	**Par.**	**Unit**	**Value**	**SE (%)**	**Value**	**SE (%)**
Dyn CC AA	e	-	0.026	0.00228	0.0114	11.6
Gomp AA	$IC_{50,AA}$	$\mu g/mL$	10.8	0.00205	10.5	6.68
Power Law AA	$IC_{50,AA}$	$\mu g/mL$	5.31	0.00142	0.919	0.217
Simeoni AA	$IC_{50,AA}$	$\mu g/mL$	2.98	0.000688	2.12	0.0485

Table 3.10: Efficacy parameters obtained from the fits of the two groups separately.

The good match between the predicted curve of Simeoni AA TGI model and the observed data confirms its predictive capabilities. This result is in agreement with the ones obtained in tumor xenograft experiments of DU145 cell line (prostate cancer) following the administration of another drug (bevacizumab) in [Rocchetti et al., 2013].

Conclusion

In the first part of this study, we had an unexpected result: the two parameters model Power Law had a significant better performance than the Gompertz V_0 (3 parameters model) describing the untreated breast tumor growth. As expected, the Gompertz V_0 despite its identifiability issue has a bigger descriptive power than Gompertz. Thus, we selected the last one as it offers identifiable parameters. At last, the Exponential-Linear and the Dynamic CC had satisfactory results. These results indicate that even with the inherent simplifications of the underlying biology, it is possible to find simple models which match closely the evolution of the tumor growth without treatment.

Computing the PK parameters from pharmacological experiments allowed us to have a precise model which describes sunitinib concentration dynamic in mice. It provides an important information helping us to focus on the drug efficacy. The AA models are sensitive to small sunitinib plasma concentration and that the drug has a fast elimination.

Thanks to the data from treated animals, we elected the Simeoni AA TGI as the model able to capture the AA treatments dynamic. The Gompertz AA TGI, the Power law AA TGI and the Dynamic CC AA failed to depict the treated curves whereas the Simeoni AA TGI succeeded to describe treated breast tumor under two different schedulings. The Simeoni AA TGI also has a significant predictive power on tumor growth following different protocols of sunitinib administration. Indeed, the prediction of the growth dynamic of the group *breastsub31* using *breastsub32* efficacy parameter and untreated growth parameters was in agreement with the observations. This study confirms the results obtained by Rocchetti for another cell line.

After studying all models on the primary tumor growth with or without treatment, one can start testing these models on experiments data which take the metastasis evolution into account using the transport equation (see equation 1.1).

Our study shows that in the case of the Simeoni AA TGI, we can learn after a single experiment the model parameters. This offers the possibility of proceeding several *in silico* experiments testing the drug influence under different schedulings in order to propose simulations for a confirmatory study. It is very useful as the preclinical experiments are expensive and hard to realize.

Appendix A

Annexes

A.1 Anti-Angiogenic therapy in Hahnfeldt model

The AA therapy is integrated in the vascularization equation through a negative term as following:

$$\frac{d}{dt}K(t) = cV(t) - dV(t)^{\frac{2}{3}}K(t) - e_{AA}C(t)K(t)$$

with $C(t)$ the plasma concentration of the drug and e_{AA} the efficacy parameter.

To integrate the pharmacokinetic of the studed drugs Hahnfeld and al considered an one-compartment model (see Figure 3.1). As anti-angiogenic drugs were intravenous administered, one single dose respect the equation 3.2. The drug concentration in an sustained therapy is given by:

$$C(t) = D\sum_{i=1}^{N} e_{AA}^{-k(t-t_i)}\mathbb{1}_{t\geq t_i}$$

with D the administrated dose which is given as bolus at times t_i and k its elimination rate.

Using the parameters they calculated (see TableA.1), we reproduced the simulations of the volume and the vascularization following different schedulings of the tree AA compounds: edostatin and angiostatin (endogenous inhibitors) and TNP-470 (exogenous inhibitor).

	TNP-470	Endostatin	Angiostatin
e_{AA} $(day^{-1}conc^{-1})$	1.3	0.66	0.15
k (day^{-1})	10.1	1.7	0.38

Table A.1: Pharmacodynamic and pharmacokinetic parameters from [Hahnfeldt et al., 1999]

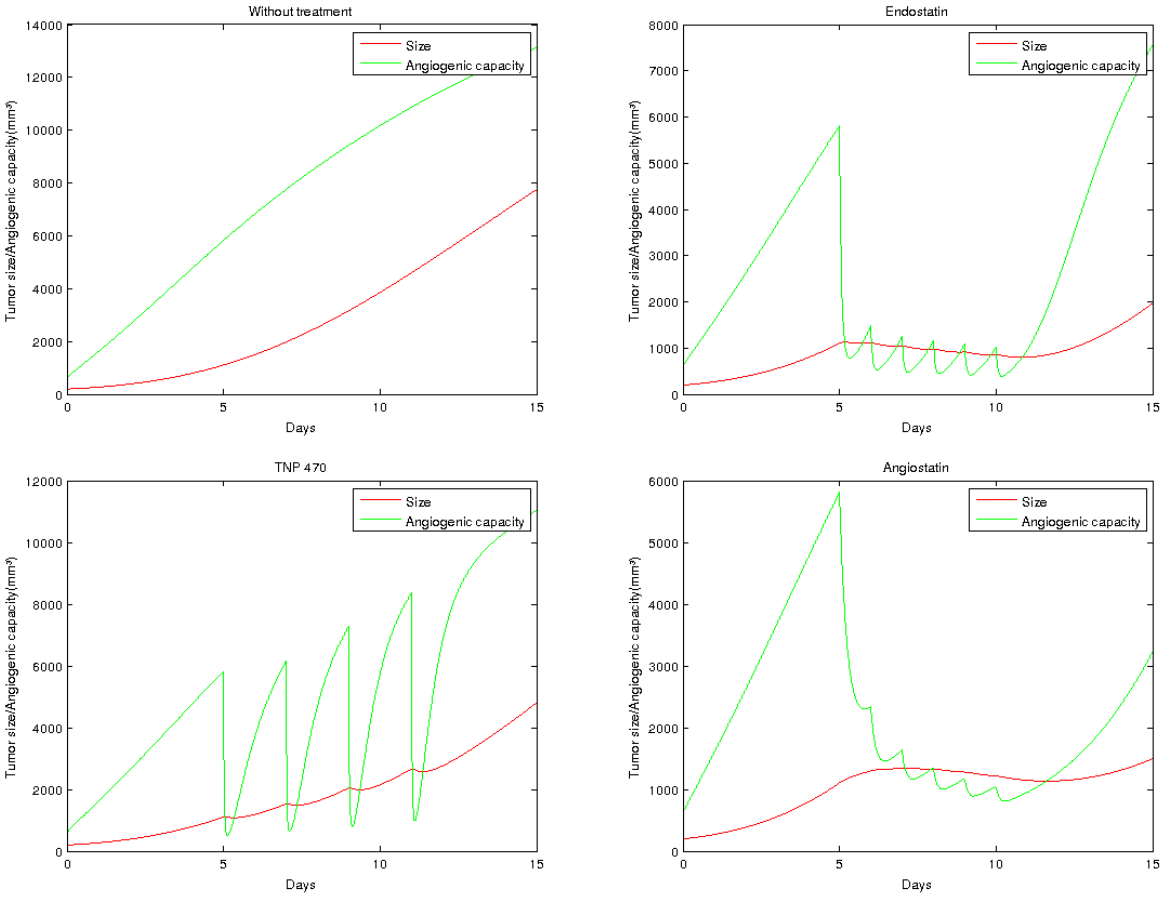

Figure A.1: Different treatments with $x_0 = 200mm^3$. The therapy is administrated from days 5 to 10 (11 for TNP-470). Endostatin: 20mg/day; TNP-470: 30mg/2 days; Angiostatin: 20mg/day.

A.2 Confrontation of numerical models to optimize an ODE resolution

Euler vs Runge Kutta 4 in untreated curves

We are looking for a good numerical method which computes with a good efficacy the solution of our PDE system that will be solved like a ODE one using the caractheristics method. For that, we compare the Euler and the Runge-Kutta 4 methods solving the ODE system proposed by Hahnfeldt (see Equation (3.1)).

We use the parameters values obtained in [Hahnfeldt et al., 1999] from fits to data on mice bearing Lewis Lung carcinoma (See Table A.2) and human parameters that were identified from data on a hepatocellular carcinoma (See Table A.3) [Iwata et al., 2000].

To evalute those methods, we use the relative error given by this expression:

$$\text{Relative Error} = \max \frac{\widetilde{|u_i - u_i|}}{u_i}$$

Where $\widetilde{u_i}$ and u_i are the numeric and the exact solution at the i^{th} interaction over N.

Remark: I take the solution given by the Runge-Kutta method with a time step very small $h = 1.e^{-5}$ as the "exact solution".

a	c	d	θ_0	α
0.192	5.85	0.00873	625	2/3
day^{-1}	day^{-1}	$day^{-1}mm^{-2}$	mm^3	

Table A.2: Values of the growth and metastatic parameters for mice. Parameters a, c and d were fitted on mice data in [Hahnfeldt et al., 1999].

a	c	d	θ_0	α
0.0042	1	$5.7251.10^{-4}$	2630.14	2/3
day^{-1}	day^{-1}	$day^{-1}mm^{-2}$	mm^3	

Table A.3: Values of the growth and metastatic parameters for human. a and α are from [Iwata et al., 2000].

Study with mice parameters for different time intervals ($h = 0.1$)

	T = 30	T = 100
Elapsed time Euler	0.0116s	0.0303s
R. E. Euleur V	0.0913	0.0913
R. E. Euler K	0.0632	0.0632
Elapsed time R.K	0.0275s	0.0920s
R. E. RK V	$1.0081.10^{-6}$	$1.0081.10^{-6}$
R. E. RK K	$4.7602.10^{-7}$	$4.7602.10^{-7}$

We see that at $T = 30$ the tumor size is smaller than the maximal reachable size limit $b = (\frac{c}{d})^{\frac{3}{2}}$ but it is reached before $T = 100$.

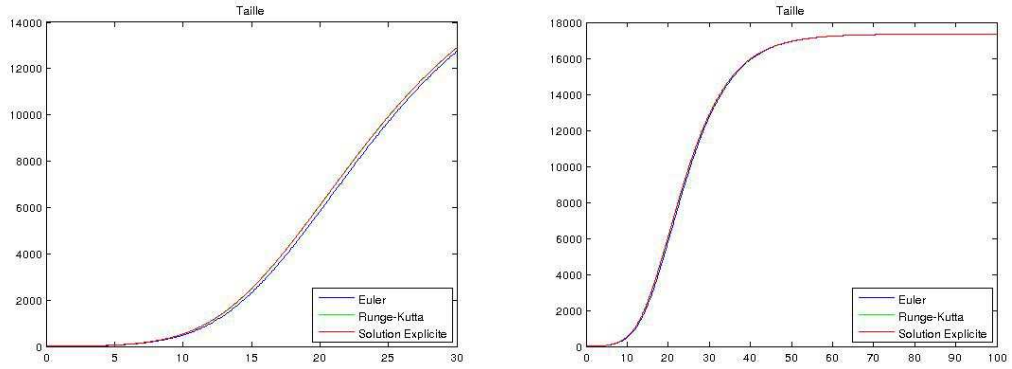

Figure A.2: Tumor evolution for time intervals $T = 30$ and $T = 100$.

Study with mice parameters for different time steps ($T = 70$)

	h=0.1	h=0.05	h=0.01	h=0.001
Elapsed time Euler	0.0219s	0.0364s	0.1451s	1.4093s
R. E. Euleur V	0.0913	0.0471	0.0097	$9.7128.10^{-4}$
R. E. Euler K	0.0632	0.0323	0.0066	$6.6196.10^{-4}$
Elapsed time R.K	0.0638s	0.1247s	0.6271s	6.2241s
R. E. RK V	$1.0081.10^{-06}$	$6.5549.10^{-08}$	$1.0825.10^{-10}$	$2.6058.10^{-14}$
R. E. RK K	$4.7602.10^{-7}$	$3.0827.10^{-08}$	$5.0730.10^{-11}$	$1.8104.10^{-14}$

Study with human parameters for different time intervals ($h = 0.1$)

	T=100	T=1000
Elapsed time Euler	0.0306s	0.2053s
R. E. Euleur V	0.0025	0.0035
R. E. Euler K	$2.9217.10^{-4}$	0.0019
Elapsed time R.K	0.0982s	0.8663s
R. E. RK V	$7.7771.10^{-13}$	$7.7771.10^{-13}$
R. E. RK K	$9.5699.10^{-14}$	$6.4977.10^{-13}$

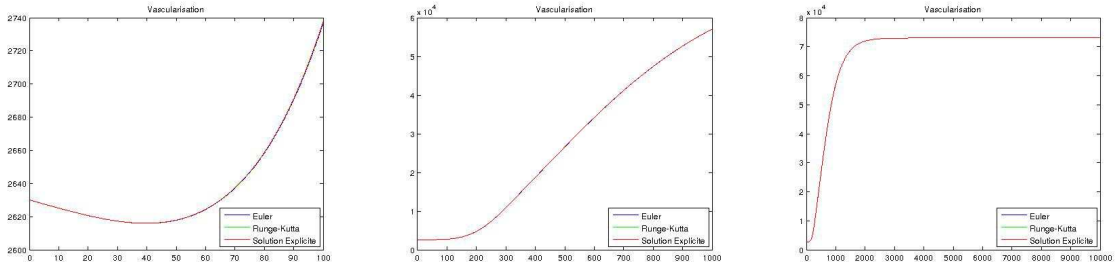

Figure A.3: Evolution of the tumor vascularization for time intervals $T = 100$ and $T = 1000$

Study with human parameters for different time steps ($T = 100$)

	h=0.1	h=0.01	h=0.001
Elapsed time Euler	0.0306s	0.2095s	1.9931s
R.E. Euleur V	0.0025	$2.5156.10^{-4}$	$2.5162.10^{-5}$
R.E. Euler K	$2.9217.10^{-4}$	$2.9292.10^{-5}$	$2.9300.10^{-6}$
Elapsed time R.K.	0.0982s	0.8736s	8.8732s
R.E. RK V	$7.7771.10^{-13}$	$5.3125.10^{-14}$	$6.4462.10^{-14}$
R.E. RK K	$9.5699.10^{-14}$	$6.7254.10^{-14}$	$9.1676.10^{-14}$

Conclusion

From the study with mice parameters for different time steps where $T = 70$ (see A.2), the best time step to compute a solution of the mentioned ODE in an untreated mice is $h = 0.1$ for the Runge-Kutta method and $h = 0.01$ for the Euler method because their Relative Error is smaller than 1%.

Euler vs Runge Kutta 4 in treated curves

Study with mice parameters for different time steps ($T = 15$)

We can not use $h = 0.1$ to solve the ODE because our solutions are not smooth. Even with a Runge-Kutta method (see Figure A.1) for which we find a relative error of 25% to the Angiogenic capacity.

Endostatin

	h=0.05	h=0.01	h=0.005	h=0.001
Elapsed time Euler	0.0153s	0.0449s	0.0982s	0.4639s
R.E. Euleur V	0.0882	0.0162	0.0080	0.0016
R.E. Euler K	0.4730	0.0852	0.0421	0.0082
Elapsed time R.K	0.0306s	0.1649s	0.2960s	1.4679s
R.E. Rk V	0.0163	0.0031	0.0015	$2.8240.10^{-04}$
R.E. Rk K	0.1212	0.0242	0.0120	0.0022

TNP 470

	h=0.05	h=0.01	h=0.005	h=0.001
Elapsed time Euler	0.0167s	0.0541s	0.0995s	**0.4589s**
R.E. Euleur V	0.1267	0.0403	0.0196	**0.0038**
R.E. Euler K	4.9633	0.3174	0.1566	**0.0306**
Elapsed time R.K	0.0474s	0.2075s	**0.4116s**	2.0458
R.E. Rk V	0.0363	0.0059	**0.0029**	$5.2805.10^{-04}$
R.E. Rk K	0.3328	0.0665	**0.0329**	0.0038

Angiostatin

	h=0.05	h=0.01
Elapsed time Euler	0.0147s	0.0405s
R.E. Euleur V	0.0254	0.0050
R.E. Euler K	0.0639	0.0122
Elapsed time R.K	0.0385s	0.1532s
R.E. Rk V	0.0054	0.0011
R.E. Rk K	0.0292	0.0058

Conclusion

As we can see, the fastest method (with a good h) is treatment-dependant. However, the method with the best satisfactory performance is the Runge-Kutta with $h = 0.005$.

Bibliography

[Benzekry, 2011] Benzekry, S. (2011). Mathematical and numerical analysis of a model for anti-angiogenic therapy in metastatic cancers. *ESAIM: M2AN*, 46(2):207–237.

[Benzekry et al., 2014a] Benzekry, S., Ebos, J., and Hahnfeldt, P. (2014a). Metastatic dynamics and systemic inhibition of angiogenesis - Implications for dormancy and surgery.

[Benzekry et al., 2014b] Benzekry, S., Lamont, C., Beheshti, A., Tracz, A., and Ebos, J. (2014b). Classical Mathematical Models for Description and Prediction of Experimental Tumor Growth. *PLoS Comput Biol*.

[Ebos et al., 2009] Ebos, J. M. L., Lee, C. R., Cruz-Munoz, W., Bjarnason, G. A., Christensen, J. G., and Kerbel, R. S. (2009). Accelerated metastasis after short-term treatment with a potent inhibitor of tumor angiogenesis. *Cancer Cell*, 15(3):232–239.

[Ebos et al., 2014] Ebos, J. M. L., Mastri, M., Lee, C. R., Tracz, A., Hudson, J. M., Attwood, K., Cruz, W. R., Jedeszko, C., Burns, P., and Kerbel, R. S. (2014). Neoadjuvant antiangiogenic therapy reveals contrasts in primary and metastatic efficacy. *Submitted*.

[Folkman, 1971] Folkman, J. (1971). Tumor angiogenesis: therapeutic implications. *N. Engl. J. Med.*, 285:1182–1186.

[Gunaratna, 2001] Gunaratna (2001). Drug Metabolism and Pharmacokinetics in Drug Discovery: A Primer For Bioanalytical Chemists, Part II. *Current separations*, 19(3):87–92.

[Gupta and Massagué, 2006] Gupta, G. P. and Massagué, J. (2006). Cancer metastasis: building a framework. *Cell*, 127(4):679–695.

[Hahnfeldt et al., 1999] Hahnfeldt, P., Panigraphy, D., Folkman, J., and Hlatky, L. (1999). Tumor development under angiogenic signaling: a dynamical theory of tumor growth, treatment, response and postvascular dormancy. *Cancer Res*, 59(19):4770–4775.

[Haznedar et al., 2009] Haznedar, J. O., Patyna, S., Bello, C. L., Peng, G. W., Speed, W., Yu, X., Zhang, Q., Sukbuntherng, J., Sweeny, D. J., Antonian, L., and Wu, E. Y. (2009). Single- and multiple-dose disposition kinetics of sunitinib malate, a multitargeted receptor tyrosine kinase inhibitor: comparative plasma kinetics in non-clinical species. *Cancer Chemother Pharmacol*, 64(4):691–706.

[Iwata et al., 2000] Iwata, K., Kawasaki, K., and Shigesada, N. (2000). A dynamical model for the growth and size distribution of multiple metastatic tumors. *J Theor Biol*, 203(2):177–186.

[O'Reilly et al., 1994] O'Reilly, M. S., Holmgren, L., Shing, Y., Chen, C., Rosenthal, R. A., Moses, M., Lane, W. S., Cao, Y., Sage, E. H., and Folkman, J. (1994). Angiostatin: a novel angiogenesis inhibitor that mediates the suppression of metastases by a Lewis lung carcinoma. *Cell*, 79(2):315–28.

[Rocchetti et al., 2013] Rocchetti, M., Germani, M., Bene, F., Poggesi, I., Magni, P., Pesenti, E., and Nicolao, G. (2013). Predictive pharmacokinetic–pharmacodynamic modeling of tumor growth after administration of an anti-angiogenic agent, bevacizumab, as single-agent and combination therapy in tumor xenografts. *Cancer Chemother Pharmacol*, 71(5):1147–1157.

[Simeoni et al., 2004] Simeoni, M., Magni, P., Cammia, C., De Nicolao, G., Croci, V., Pesenti, E., Germani, M., Poggesi, I., and Rocchetti, M. (2004). Predictive pharmacokinetic-pharmacodynamic modeling of tumor growth kinetics in xenograft models after administration of anticancer agents. *Cancer Res*, 64(3):1094–1101.